Inorganic Chemistry

pubs.acs.org/IC Article

Antiferromagnetism of Double Molybdate $LiFe(MoO_4)_2$

Meifeng Liu, Yang Zhang, Tao Zou,* V. Ovidiu Garlea, Timothy Charlton, Yu Wang, Fei Liu, Yunlong Xie, Xiang Li, Lun Yang, Biwen Li, Xiuzhang Wang, Shuai Dong,* and Jun-Ming Liu

Cite This: *Inorg. Chem.* 2020, 59, 8127−8133 Read Online

ACCESS | Metrics & More | Article Recommendations | Supporting Information

ABSTRACT: The magnetic properties of the spin-5/2 double molybdate $LiFe(MoO_4)_2$ have been characterized by heat capacity, magnetic susceptibility, and neutron powder diffraction techniques. Unlike the multiferroic system $LiFe(WO_4)_2$ which exhibits two successive magnetic transitions, $LiFe(MoO_4)_2$ undergoes only one antiferromagnetic transition at $T_N \sim 23.8$ K. Its antiferromagnetic magnetic structure with the commensurate propagation vector $\mathbf{k}$ = (0, 0.5, 0) has been determined. Density functional theory calculations confirm the antiferromagnetic ground state and provide a numerical estimate of the relevant exchange coupling constants.

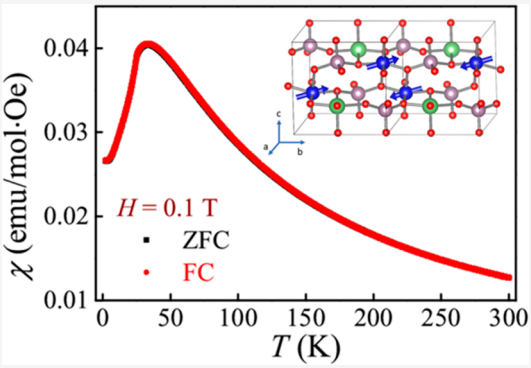

Downloaded via SOUTHEAST UNIV on June 16, 2020 at 05:46:31 (UTC).
See https://pubs.acs.org/sharingguidelines for options on how to legitimately share published articles.

I. INTRODUCTION

Double tungstates and molybdates with the chemical formula $A^IB^{III}(MO_4)_2$ form a big family of transition metal oxides, where A is an alkali metal; B is a trivalent cation such as Bi^{3+}, In^{3+}, or Fe^{3+} or a rare earth, Sm^{3+} or Eu^{3+}; and M represents W^{6+} or Mo^{6+}.[1−5] The combinations of three categories of metal ions make this family full of varieties in physics and functionality. The inclusion of the Li ion at A site makes them suitable to be used in lithium-ion batteries as anode materials, while the W/Mo can provide a relative large spin−orbit coupling considering its 4d/5d orbitals.[1,6−9] Most importantly, the B-site ions with narrow bands can provide other applicable physical properties, such as magnetism and luminescence.[10−15]

Recently, $NaFe(WO_4)_2$ was reported to exhibit an incommensurate spiral spin order at low temperature (<4 K),[16] although this magnetism can not induce a net ferroelectric (FE) polarization (P) due to the opposite chirality coexisting in this material. Differently, Liu et al. revealed a more interesting magnetic spiral in $LiFe(WO_4)_2$, which breaks the spatial reversal symmetry and induces a net FE P along the [010] axis below 19.7 K through the inverse Dzyaloshinskii−Moriya (DM) interaction.[17] Thus, $LiFe(WO_4)_2$ is the second experimentally confirmed multiferroic material in the tungstate family, following the first one $MnWO_4$.[18,19] Despite the common chemical formula, the crystalline structures of double tungstates/molybdates can vary in a large range. In fact, $LiFe(WO_4)_2$ and $NaFe(WO_4)_2$ are different in their space groups ($C2/c$ vs $P2/m$), and the arrangements of Fe ions are distinct. Such structural diversity makes it is possible to find more exotic magnetic properties in double tungstates/molybdates. For instance, it was reported that $RbFe(MoO_4)_2$ possesses a noncollinear magnetic order below 3.8 K which can trigger the ferroelectricity.[20] In addition, there are lots of other tungstates/molybdates members, e.g., $FeWO_4$, $CoWO_4$, $NiWO_4$, $CuWO_4$, α-$FeMoO_4$, α-$CoMoO_4$, and $NaCr(WO_4)_2$, all of which display collinear antiferromagnetic orders and thus are not ferroelectric.[21−25] Recently, Chen et al. synthesized $LiFe(MoO_4)_2$ and investigated it for its applications in lithium-ion batteries.[6] Distinct from either $LiFe(WO_4)_2$ or $NaFe(WO_4)_2$, $LiFe(MoO_4)_2$ possesses a new space group $P\bar{1}$ and another type of Fe framework. Its excellent electrochemical properties have been carefully studied. Nevertheless, its magnetic properties have never been studied yet.

In this work, we will report the magnetism of $LiFe(MoO_4)_2$ determined from combined studies of heat capacity, magnetic susceptibility, neutron powder diffraction, as well as density functional theory (DFT) calculation. An antiferromagnetic (AFM) phase transition is found around 23.8 K. Below the Néel temperature (T_N), a long-range magnetic ordering is established with a commensurate propagation vector (0, 0.5, 0), which does not yield multiferroicity. Above T_N, short-range magnetic correlation persists, leading to considerable magnetic entropy.

Received: February 11, 2020
Published: June 2, 2020

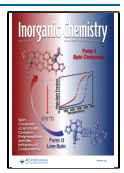

ACS Publications © 2020 American Chemical Society

II. METHODS

High-quality polycrystalline $LiFe(MoO_4)_2$ samples were synthesized using the conventional solid state reaction method in air, with the highly purified powder of oxides and carbonates as starting materials. The stoichiometric mixtures were ground and fired at 550 °C for 24 h in air. The resultant powder was reground and pelletized under a pressure of 1000 psi into disks of 2.0 cm in diameter, and then, these pellets were sintered at 650 °C for 24 h in air again. Phase purity of the sample was checked using X-ray diffraction (XRD) with the Cu Kα radiation at room temperature. The magnetic properties were measured using a superconducting quantum interference device magnetometer (SQUID) equipped on a quantum design magnetometer (MPMSXL-7). The specific heat was measured on the physical property measurement system (PPMS, Quantum Design) using the heat relaxation method. Neutron powder diffraction (NPD) patterns were collected with neutron wavelength λ = 2.41 Å at the HB-2A powder diffractometer at the High Flux Isotope Reactor, Oak Ridge National Laboratory.

DFT calculations were performed using the Vienna *ab initio* simulation package (VASP) with the projector augmented-wave (PAW) potentials.[26−28] The Perdew−Burke−Ernzerhof for solids (PBEsol) exchange function has been adopted[29] to obtain an accurate description of the crystal structure of $LiFe(MoO_4)_2$. The Hubbard U_{eff} (=$U - J$) was imposed on Fe's d orbitals using the Dudarev implementation[30] considering the strong correlation effect of 3d orbitals. No U_{eff} is applied to Mo's 4d orbitals considering its empty occupation and weaker correlation comparing with 3d orbitals. The cutoff energy of the plane wave basis was fixed to 650 eV due to a quite high convergent value of Li. The Brillouin zone was adopted using 6 × 6 × 3 Monkhorst−Pack *k*-point mesh for the minimal magnetic unit cell. Besides, both the lattice constants and atomic positions were fully relaxed until the Hellmann−Feynman force on each atom is below 0.01 eV/Å.

III. RESULTS AND DISCUSSION

Figure 1a shows the crystal structure of $LiFe(MoO_4)_2$, which is described in the triclinic space group $P\bar{1}$ (No. 2) and consisted of separated layers of $[LiO_6]$ monocapped trigonal bipyramids, $[FeO_6]$ octahedra, and $[MoO_4]$ tetrahedra. The framework of magnetic Fe ions in $LiFe(MoO_4)_2$ is shown in Figure 1b.

Figure 1c shows the powder XRD pattern of $LiFe(MoO_4)_2$ at room temperature. The lattice parameters were refined using the space group $P\bar{1}$ with the Rietveld refinement technique. No impurity phase is observed in the XRD power pattern. The refined lattice parameters of $LiFe(MoO_4)_2$ are a = 6.7766 Å, b = 7.1679 Å, c = 7.3104 Å, α = 90.89°, β = 110.38°, and γ = 105.21°, which are in good consistency with previous works.[31,32]

Besides XRD, NPD data of $LiFe(MoO_4)_2$ were collected at T = 40 K, as shown in Figure 1d. The nuclear structure refinement was conducted using FullProf with the Rietveld method.[26] Our refinement confirms that the compound possesses a triclinic structure with the space group $P\bar{1}$. No impurity phase was detected. The corresponding lattice parameters are a = 6.751(1) Å, b = 7.203(2) Å, c = 7.1702(1) Å, α = 90.6739(17)°, β = 110.2274(14)°, and γ = 105.5793(17)°, in agreement with above XRD results. Table 1 summarizes more parameters such as atomic coordinates and displacement parameters.

Figure 2a depicts the magnetic susceptibility (χ) and its inverse ($1/\chi$) as a function of temperature (T) measured following zero field cooling (ZFC) and field cooling (FC) processes at a 0.1 T field. The two curves almost overlap, and no bifurcation is seen in the whole temperature range, suggesting the absence of glass behavior. A peak of $d\chi/dT$ was observed around T_N ~ 23.8 K, indicating the establishment of long-range magnetic ordering, as shown in the inset of Figure 2b. The χ(T) of $LiFe(MoO_4)_2$ can be well fitted to the Curie−Weiss law $\chi = C/(T - \theta_{CW})$, as also shown in Figure 2a. Our fitting in the temperature range between 100 and 300 K yields the Curie constant C ~ 4.53 emu K/mol and negative Curie−Weiss temperature θ_{CW} ~ −52.85 K, suggesting dominant AFM interactions between Fe's spins. The effective moment per Fe^{3+} of 6.02 μ_B is very close to spin-only moment (5.92 μ_B) for high-spin Fe^{3+} (S^z = 5/2, L = 0).

Figure 2b shows the magnetic susceptibility under a high magnetic field (6 T). There is a maximum of χ at T_{max} ~ 32.8 K, which may due to the ordering of short-range magnetic

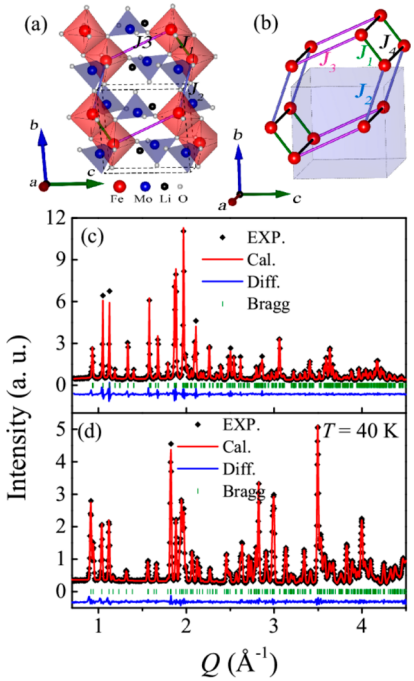

Figure 1. (a) Projection in the *bc* plane of the crystal structure of $LiFe(MoO_4)_2$. Red, Fe; blue, W; black, Li; gray, O. (b) Framework of Fe ions and the magnetic exchange paths $J_1/J_2/J_3$. (c) XRD pattern measured at room T and the corresponding Rietveld fit. (d) Neutron powder diffraction pattern collected at 40 K with a neutron wavelength of λ = 2.41 Å.

Table 1. Refined Structural Parameters of $LiFe(MoO_4)_2$ from Neutron Powder Diffraction Data Collected at 40 K with the Neutron Wavelength of λ = 2.41 Å[a]

atom (Wyck.)	x	y	z	B
Mo1 (2i)	0.3326(4)	0.5768(2)	0.2907(3)	0.071(3)
Mo2 (2i)	0.8221(6)	−0.0395(5)	0.2272(5)	0.071(3)
Fe (2i)	0.4001(4)	0.0996(4)	0.317 52(4)	0.073(4)
Li (2i)	0.7580(2)	0.4418(2)	0.2557(2)	0.803(2)
O1 (2i)	0.4166(7)	0.8407(73)	0.3907(6)	0.342(2)
O2 (2i)	0.2563(5)	0.5731(65)	0.039 78(6)	0.342(2)
O3 (2i)	0.0891(7)	0.4879(60)	0.3351(6)	0.342(2)
O4 (2i)	0.4795(6)	0.3805(63)	0.3539(6)	0.342(2)
O5 (2i)	0.6896(7)	0.1301(63)	0.2682(7)	0.342(2)
O6 (2i)	0.7755(6)	−0.0499(70)	−0.0271(6)	0.342(2)
O7 (2i)	0.7082(6)	−0.2787(60)	0.2690(9)	0.342(2)
O8 (2i)	1.1138(6)	0.0417(63)	0.358 52(6)	0.342(2)

[a]Space group: $P\bar{1}$, a = 6.751(1) Å, b = 7.203(2) Å, c = 7.1702(1) Å, α = 90.6739(17)°, β = 110.2274(14)°, γ = 105.5793(17)°, R_p = 3.00%, R_{wp} = 5.61%.

https://dx.doi.org/10.1021/acs.inorgchem.0c00432
Inorg. Chem. 2020, 59, 8127−8133

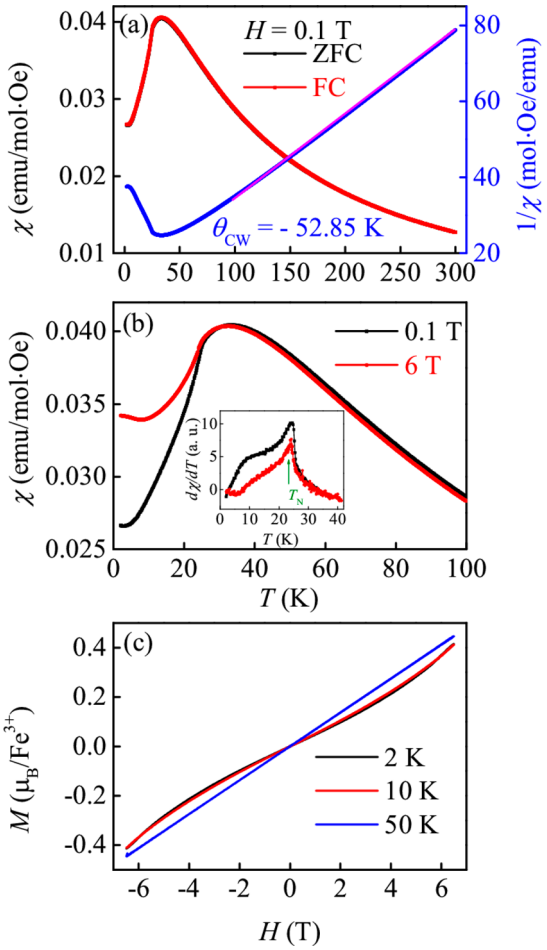

Figure 2. (a) Temperature dependence of magnetic susceptibility (left *y*-axis) and its inverse (right *y*-axis) of $LiFe(MoO_4)_2$ measured under a 0.1 T field. (b) Temperature evolution of magnetic susceptibility under various magnetic fields. The inset shows the amplified view of the derivatives of χ around the phase transition temperature. (c) Moment size of the Fe^{3+} ion as a function of magnetic field at various temperatures.

correlation for this low-dimensional spin system. The peak of $d\chi/dT$ appears near $T_N \sim 23.8$ K, in agreement with aforementioned long-range AFM magnetic ordering (LRO). In addition, Figure 2c shows the magnetization (M) as a function of magnetic field (H) at various temperatures 2, 10, and 50 K. The $M(H)$ curves below T_N show nonlinear behavior with the applied magnetic field. The largest M value is only ~0.4 μ_B/Fe when magnetic field is up to 6.5 T at 2 K, suggesting the canting AFM state under strong magnetic fields.

We also measured the T-dependence of its heat capacity (C_p), as shown in the Figure 3a. A clear λ-shaped peak was observed around $T \sim 23.8$ K, which is one more indication of the long-range magnetic ordering. Considering the fact that $LiFe(MoO_4)_2$ is an insulator, the specific heat mainly contains the contributions from both magnons and phonons. At high temperatures, C_p is fully dominated by the phonon excitation contribution. Thus, the C_p of isostructural and nonmagnetic $LiGa(MoO_4)_2$ (red curve in Figure 3a) was measured and used to subtract the phonon contribution from $LiFe(MoO_4)_2$. Then the obtained magnetic heat capacity C_M is shown in Figure 3b. The broad hump in both magnetic susceptibility and specific heat around ~10 K might originate from the temperature-

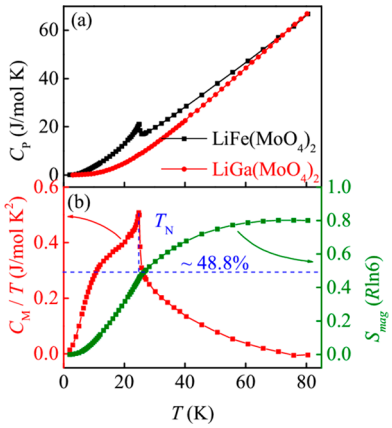

Figure 3. (a) Heat capacity of magnetic $LiFe(MoO_4)_2$ and nonmagnetic $LiGa(MoO_4)_2$ measured under 0 T magnetic field. (b) Magnetic contribution of the specific heat C_{mag} as a function of temperature acquired by subtracting the phonon contribution using nonmagnetic $LiGa(MoO_4)_2$ (left *y*-axis) and the magnetic entropy S_{mag} as a function of temperature (right *y*-axis).

dependent exchange effects. As suggested in ref 33, below T_N, the populations and energies of Zeeman levels due to the temperature-dependent exchange field would be more significant if the spin quantum number is large, as here the spin number $S = 5/2$. The magnetic entropy (S_M) is estimated through integrating C_M/T over T, giving a saturation value of $S_M \sim 11.9418$ J/(mol K) at 80 K as shown in Figure 3b. This value is very close to the calculation value of total spin entropy of $R \ln(2S + 1) = 14.897$ J/(mol K) ($R = 8.314$ J/(mol K)). The entropy gain at T_N is only ~48.8% of the total magnetic entropy, indicating the existence of short-range magnetic correlations above T_N, which is a characteristic of low-dimensional magnets.

To reveal the AFM spin structure of $LiFe(MoO_4)_2$, the NPD pattern was collected at 1.5 K. As shown in Figure 4b, a series of new Bragg peaks indicated by the second row of vertical bars show up compared to the data collected at 40 K. The inset displays a zoomed view of the low-Q region to show the peaks more clearly. No obvious change of lattice parameters was observed. In Figure 4c, the difference between the 40 and 1.5 K patterns clearly shows the details of these magnetic Bragg peaks. The observed magnetic peaks can be well indexed with a commensurate propagation vector $\mathbf{k} = (0, 0.5, 0)$, distinct from the incommensurate one $\mathbf{k} = (0.890, 0, 0.332)$ seen in $LiFe(WO_4)_2$ and a noncollinear triangular spin order seen in $RbFe(MoO_4)_2$.

Figure 4a exhibits the temperature evolution of the peak intensity of the (0, −0.5, 1) magnetic Bragg peak. A fit to the power law $I = A(T_c - T)^{2\beta}$ over the temperature range 8−29 K yields $T_c = 24.1(2)$ K and a critical exponent $\beta = 0.218$. The obtained β is close to the expected value for the 2D-XY model (~0.23) expected for layered magnetic structures.[34]

Representation analysis constrains the possible magnetic structures to the basis vectors associated with an irreducible representation (IR) of the crystal space group and $\mathbf{k} = (0, 0.5, 0)$. We used *SARAh* software to perform the analysis on magnetic Fe^{3+} ions. There are two possible irreducible representation allowed for the Fe^{3+} ion at the 2*i* Wyckoff position, corresponding to Γ_1 and Γ_2 in the Kovalev numbering scheme, as listed in Table 2. Three basis vectors are allowed for each representation. While the Γ_1 is ruled out since it cannot

https://dx.doi.org/10.1021/acs.inorgchem.0c00432
Inorg. Chem. 2020, 59, 8127−8133

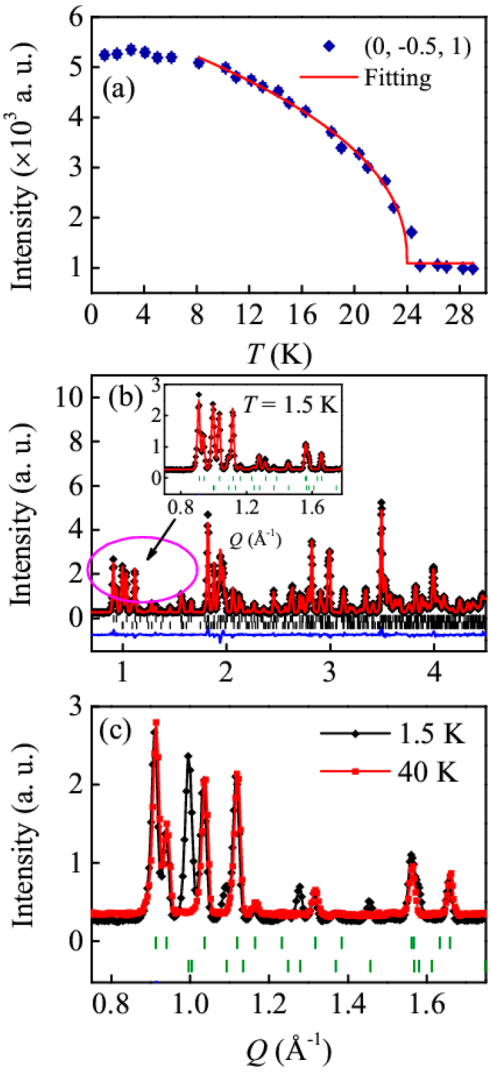

Figure 4. (a) Temperature evolution of the (0, −0.5, 1) magnetic Bragg peak. (b) Neutron powder diffraction pattern collected at 1.5 K with a neutron wavelength of λ = 2.41 Å. The inset shows the enlarged area of the low Q region to clearly exhibit the magnetic Bragg peaks. (c) Comparison of neutron powder diffraction patterns collected at 1.5 and 40 K.

Table 2. Basis Vectors for the Space Group $P\bar{1}$ with the Propagation Vector k = (0, 0.5, 0)[a]

IR	BV	Fe1 (0.4027, 0.102, 0.318)	Fe2 (0.597, 0.897, 0.682)
Γ_1	ψ_1	(1, 0, 0)	(−1, 0, 0)
	ψ_2	(0, 1, 0)	(0, −1, 0)
	ψ_3	(0, 0, 1)	(0, 0, −1)
Γ_2	ψ_4	(1, 0, 0)	(1, 0, 0)
	ψ_5	(0, 1, 0)	(0, 1, 0)
	ψ_6	(0, 0, 1)	(0, 0, 1)

[a]The decomposition of the magnetic representation for the Fe site (0.4027, 0.102, 0.318) is $\Gamma_{Fe} = 3\Gamma_1 + 3\Gamma_2$. The atoms of the nonprimitive basis are defined according to 1, (0.4027, 0.102, 0.318); 2, (0.597, 0.897, 0.682).

reproduce the correct magnetic intensities, the Γ_2 spin model gives us good fitting results as shown in Figure 4b. The corresponding magnetic structure is presented in Figure 5 with the refined amplitude of the magnetic moment 4.23(1) μ_B. The projections of the moment on the crystallographic axes are

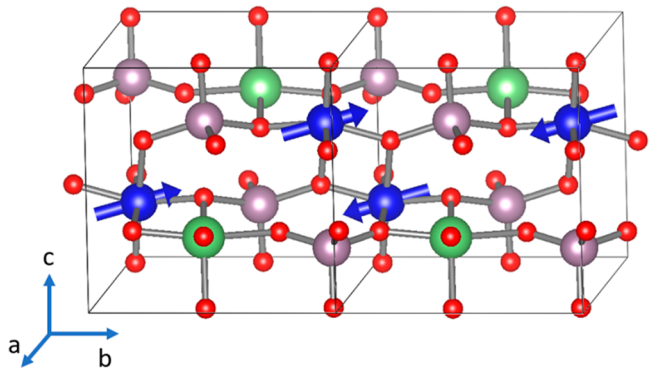

Figure 5. Magnetic structure of $LiFe(MoO_4)_2$ determined from the neutron diffraction patterns.

(m_a, m_b, m_c) = (0.582, 4.2, 1.296) μ_B. This value is only slightly smaller than the expected value for the spin S = 5/2, but it is still reasonable considering the low-dimensionality magnetic interactions.

To further understand the magnetic properties, DFT calculations have been performed. Various possible magnetic arrangements were checked, such as ferromagnetic (FM), AF1−AFM, AF2−AFM, and AF3−AFM, as shown in Figure 6.

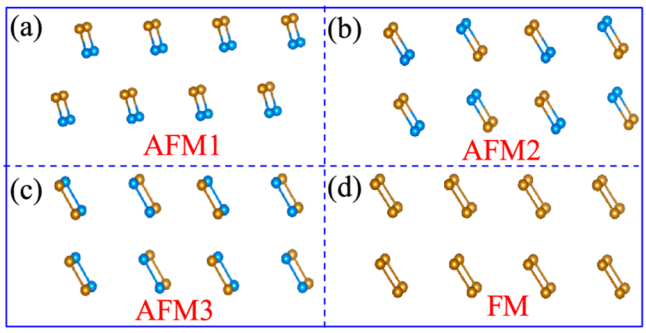

Figure 6. Sketch of possible spin configurations in the $LiFe(MoO_4)_2$ lattice.

As shown in Figure 7, the AF2−AFM configuration has the lowest energy despite the choice of U_{eff}, in agreement with our neutron experimental result. The calculated local magnetic moment of the AF2−AFM state is 4.22 μ_B/Fe at U_{eff} = 4 eV, which is quite close to our neutron experiments (4.23 μ_B/Fe). In fact, U_{eff} = 4 eV is a proper choice to describe Fe's 3d orbitals according to previous studies,[17,35] which will be adopted as the default one. The optimized lattice constants of the AF2−AFM state are a = 6.748 Å, b = 7.233 Å, and c = 7.113 Å, which are quite close to our neutron experiments (a = 6.751 Å, b = 7.203 Å, c = 7.1702 Å at 1.5 K).

Furthermore, the magnetism of $LiFe(Mo_4)_2$ can be described using a Heisenberg model:

$$H = -J_1 \sum_{\langle ij \rangle} S_i \cdot S_j - J_2 \sum_{[kl]} S_k \cdot S_l - J_3 \sum_{\{mn\}} S_m \cdot S_n \quad (1)$$

where J_1, J_2, and J_3 are the exchange couplings (as indicated in Figure 1b) between iron spins S's. Using the optimized ground state configuration, the exchange coefficients are extracted from DFT calculations: J_1 = −18.03 meV, J_2 = 2.06 meV, and J_3 = 2.07 meV, respectively. The strongest negative exchange J_1 indicates the AFM coupling between the nearest neighbor iron spins. Those longer distance exchanges J_2 and J_3 are much

https://dx.doi.org/10.1021/acs.inorgchem.0c00432
Inorg. Chem. 2020, 59, 8127−8133

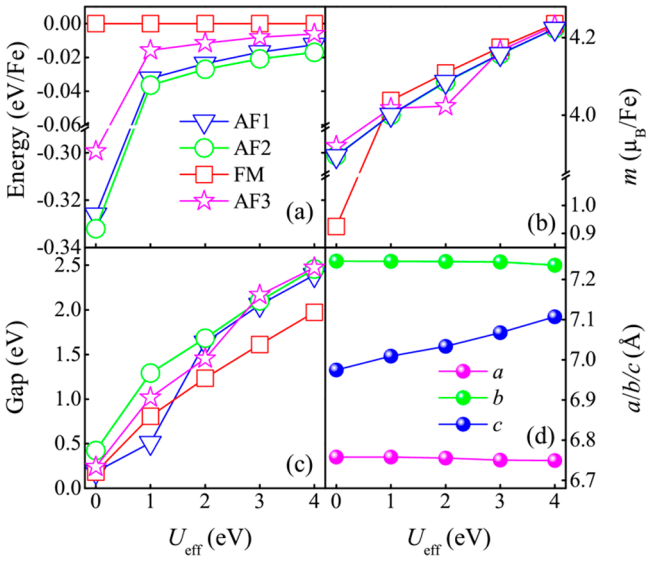

Figure 7. DFT results of single $LiFe(MoO_4)_2$ as a function of U_{eff}. (a) Energy (per Fe) of various magnetic orders. The FM state is taken as the reference. (b) Local magnetic moment of Fe calculated within the default Wigner−Seitz sphere. (c) Band gaps. (d) Relaxed lattice constants of AF2 states.

weaker: the positive J_2 implies FM interaction along the *b*-axis, and the positive J_3 means that the magnetic coupling between near iron is FM exchange. In short, our theoretical calculation confirms the magnetic ground state of $LiFe(MoO_4)_2$.

The atomic-projected density of states (DOS) of the AF2−AFM state is shown in Figure 8. It is clear that this system is an

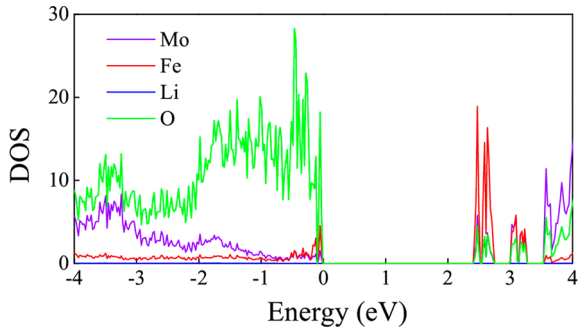

Figure 8. Atomic-projected density of states (DOS) of AF2 (U_{eff} = 4 eV). Below the Fermi level, the oxygen and irons have large overlap ranges, implying orbital hybridization.

insulator with an indirect gap of 2.46 eV. According to DOS, the topmost valence bands are mainly contributed by the hybrid O's 3p orbitals and Fe's 3d orbitals (lower Hubbard bands), while the lowest conduction bands are mainly from Fe's 3d orbitals (i.e., upper Hubbard bands). The slight reduction of local magnetic moment from the ideal 5 μ_B/Fe is due to such hybridization.

IV. CONCLUSION

In summary, the physical properties of the spin-5/2 double molybdate $LiFe(MoO_4)_2$ have been systematically investigated experimentally and theoretically. Our magnetic susceptibility and heat capacity measurements found an antiferromagnetic long-range ordering at $T_N \sim 23.8$ K, which was further confirmed by neutron diffraction. Its antiferromagnetic magnetic structure with the commensurate propagation vector **k** = (0, 0.5, 0) has also been determined. Our DFT calculations further verified the magnetic ground state. Short-range magnetic correlation was also made evident above the Néel temperature.

■ ASSOCIATED CONTENT

Supporting Information

The Supporting Information is available free of charge at https://pubs.acs.org/doi/10.1021/acs.inorgchem.0c00432.

Powder diffraction data table (PDF)

Magnetic structure file of $LiFe(MoO_4)_2$ (MCIF)

■ AUTHOR INFORMATION

Corresponding Authors

Tao Zou − *Neutron Scattering Division, Oak Ridge National Laboratory, Oak Ridge, Tennessee 37831, United States*; Email: taozoucn@gmail.com

Shuai Dong − *School of Physics, Southeast University, Nanjing 211189, China*; orcid.org/0000-0002-6910-6319; Email: sdong@seu.edu.cn

Authors

Meifeng Liu − *Institute for Advanced Materials, Hubei Normal University, Huangshi 435002, China*; orcid.org/0000-0001-5733-8764

Yang Zhang − *School of Physics, Southeast University, Nanjing 211189, China*; orcid.org/0000-0003-3623-5883

V. Ovidiu Garlea − *Neutron Scattering Division, Oak Ridge National Laboratory, Oak Ridge, Tennessee 37831, United States*

Timothy Charlton − *Neutron Scattering Division, Oak Ridge National Laboratory, Oak Ridge, Tennessee 37831, United States*

Yu Wang − *Institute for Advanced Materials, Hubei Normal University, Huangshi 435002, China*

Fei Liu − *Institute for Advanced Materials, Hubei Normal University, Huangshi 435002, China*

Yunlong Xie − *Institute for Advanced Materials, Hubei Normal University, Huangshi 435002, China*

Xiang Li − *Institute for Advanced Materials, Hubei Normal University, Huangshi 435002, China*; orcid.org/0000-0003-0671-7160

Lun Yang − *Institute for Advanced Materials, Hubei Normal University, Huangshi 435002, China*

Biwen Li − *Institute for Advanced Materials, Hubei Normal University, Huangshi 435002, China*

Xiuzhang Wang − *Institute for Advanced Materials, Hubei Normal University, Huangshi 435002, China*

Jun-Ming Liu − *Institute for Advanced Materials, Hubei Normal University, Huangshi 435002, China; Laboratory of Solid State Microstructures and Innovative Center of Advanced Microstructures, Nanjing University, Nanjing 210093, China*; orcid.org/0000-0001-8988-8429

Complete contact information is available at: https://pubs.acs.org/10.1021/acs.inorgchem.0c00432

Notes

The authors declare no competing financial interest.

https://dx.doi.org/10.1021/acs.inorgchem.0c00432
Inorg. Chem. 2020, 59, 8127−8133

■ ACKNOWLEDGMENTS

This work was supported by the National Key Research Projects of China (Grant 2016YFA0300101) and the National Natural Science Foundation of China (Grants 11704109, 11834002). The research at Oak Ridge National Laboratory's High Flux Isotope Reactor was sponsored by the Scientific User Facilities Division, Office of Basic Energy Sciences, US Department of Energy. Most calculations were supported by National Supercomputer Center in Guangzhou (Tianhe II).

■ REFERENCES

(1) Peng, N.; Cheng, X.; Yu, H.; Zhu, H.; Liu, T.; Zheng, R.; Shui, M.; Xie, Y.; Shu, J. $LiY(MoO_4)_2$ nanotubes: Novel zero-strain anode for electrochemical energy storage. *Energy Storage Materials* **2019**, *21*, 297−307.

(2) Yang, J.; Fu, P.; Lin, Z. Preparation of $KBi(MoO_4)_2$ nanocrystallite by solvothermal process and its gas-sensing properties. *Mater. Res. Express* **2018**, *5* (6), 065033.

(3) Mączka, M.; Hanuza, J.; Pietraszko, A. Vibrational and X-ray Studies of the Polymorphic Forms of $LiIn(MoO_4)_2$. *J. Solid State Chem.* **2000**, *154* (2), 498−506.

(4) Zhao, D.; Shi, J.-C.; Nie, C.-K.; Zhang, R.-J. Crystal structure and luminescent properties of two lithium lanthanide tungstate $LiLn(WO_4)_2$ (Ln = Sm, Eu). *Optik* **2017**, *138*, 476−486.

(5) Svistov, L. E.; Smirnov, A. I.; Prozorova, L. A.; Petrenko, O. A.; Demianets, L. N.; Shapiro, A. Y. Quasi-two-dimensional antiferromagnet on a triangular lattice $RbFe(MoO_4)_2$. *Phys. Rev. B: Condens. Matter Mater. Phys.* **2003**, *67* (9), 094434.

(6) Chen, N.; Yao, Y.; Wang, D.; Wei, Y.; Bie, X.; Wang, C.; Chen, G.; Du, F. $LiFe(MoO_4)_2$ as a Novel Anode Material for Lithium-Ion Batteries. *ACS Appl. Mater. Interfaces* **2014**, *6* (13), 10661−10666.

(7) Li, C.-L.; Fu, Z.-W. Electrochemical characterization of amorphous $LiFe(WO_4)_2$ thin films as positive electrodes for rechargeable lithium batteries. *Electrochim. Acta* **2008**, *53* (22), 6434−6443.

(8) Gupta, A.; Singh, P.; Mullins, C. B.; Goodenough, J. B. Investigation of Reversible Li Insertion into $LiY(WO_4)_2$. *Chem. Mater.* **2016**, *28* (13), 4641−4645.

(9) Munirathnappa, A. K.; Dwibedi, D.; Hester, J.; Barpanda, P.; Swain, D.; Narayana, C.; Sundaram, N. G. In Situ Neutron Diffraction Studies of $LiCe(WO_4)_2$ Polymorphs: Phase Transition and Structure−Property Correlation. *J. Phys. Chem. C* **2019**, *123* (2), 1041−1049.

(10) Maczka, M.; Pietraszko, A.; Saraiva, G. D.; Filho, A. G. S.; Paraguassu, W.; Lemos, V.; Perottoni, C. A.; Gallas, M. R.; Freire, P. T. C.; Tomaszewski, P. E.; Melo, F. E. A.; Filho, J. M.; Hanuza, J. High pressure effects on the structural and vibrational properties of antiferromagnetic $KFe(MoO_4)_2$. *J. Phys.: Condens. Matter* **2005**, *17* (39), 6285−6300.

(11) Zhang, J.; Wang, X.; Zhang, X.; Zhao, X.; Liu, X.; Peng, L. Microwave synthesis of $NaLa(MoO_4)_2$ microcrystals and their near-infrared luminescent properties with lanthanide ion doping (Er^{3+}, Nd^{3+}, Yb^{3+}). *Inorg. Chem. Commun.* **2011**, *14* (11), 1723−1727.

(12) Li, K.; Deun, R. V. Low-Temperature Solid-State Synthesis and Upconversion Luminescence Properties in $(Na/Li)Bi(MoO_4)_2$:Yb^{3+},Er^{3+} and Color Tuning in $(Na/Li)Bi(MoO_4)_2$:Yb^{3+},Ho^{3+},Ce^{3+} Phosphors. *Inorg. Chem.* **2019**, *58* (10), 6821−6831.

(13) Hou, L.; Cui, S.; Fu, Z.; Wu, Z.; Fu, X.; Jeong, J. H. Facile template free synthesis of $KLa(MoO_4)_2$:Eu^{3+},Tb^{3+} microspheres and their multicolor tunable luminescence. *Dalton Trans.* **2014**, *43* (14), 5382−5392.

(14) Durairajan, A.; Ramana, E. V.; Teixeira, B.; Sobolev, N.; Graça, M.; Valente, M. Magnetic and electric characterizations of sol−gel-derived $NaFe(WO_4)_2$ rods. *Appl. Phys. A: Mater. Sci. Process.* **2018**, *124* (9), 618.

(15) Nyam-Ochir, L.; Ehrenberg, H.; Buchsteiner, A.; Senyshyn, A.; Fuess, H.; Sangaa, D. The magnetic structures of double tungstates, $NaM(WO_4)_2$, M = Fe, Cr: Examples for superexchange couplings mediated by [NaO6]-octahedra. *J. Magn. Magn. Mater.* **2008**, *320* (23), 3251−3255.

(16) Holbein, S.; Ackermann, M.; Chapon, L.; Steffens, P.; Gukasov, A.; Sazonov, A.; Breunig, O.; Sanders, Y.; Becker, P.; Bohatý, L.; Lorenz, T.; Braden, M. Strong magnetoelastic coupling at the transition from harmonic to anharmonic order in $NaFe(WO_4)_2$ with $3d^5$ configuration. *Phys. Rev. B: Condens. Matter Mater. Phys.* **2016**, *94* (10), 104423.

(17) Liu, M.; Lin, L.; Zhang, Y.; Li, S.; Huang, Q.; Garlea, V. O.; Zou, T.; Xie, Y.; Wang, Y.; Lu, C.; Yang, L.; Yan, Z.; Wang, X.; Dong, S.; Liu, J.-M. Cycloidal magnetism driven ferroelectricity in double tungstate $LiFe(WO_4)_2$. *Phys. Rev. B: Condens. Matter Mater. Phys.* **2017**, *95* (19), 195134.

(18) Taniguchi, K.; Abe, N.; Takenobu, T.; Iwasa, Y.; Arima, T. Ferroelectric Polarization Flop in a Frustrated Magnet $MnWO_4$ Induced by a Magnetic Field. *Phys. Rev. Lett.* **2006**, *97* (9), 097203.

(19) Taniguchi, K.; Abe, N.; Ohtani, S.; Arima, T. Magnetoelectric Memory Effect of the Nonpolar Phase with Collinear Spin Structure in Multiferroic $MnWO_4$. *Phys. Rev. Lett.* **2009**, *102* (14), 147201.

(20) Kenzelmann, M.; Lawes, G.; Harris, A. B.; Gasparovic, G.; Broholm, C.; Ramirez, A. P.; Jorge, G. A.; Jaime, M.; Park, S.; Huang, Q.; Shapiro, A. Y.; Demianets, L. A. Direct Transition from a Disordered to a Multiferroic Phase on a Triangular Lattice. *Phys. Rev. Lett.* **2007**, *98* (26), 267205.

(21) Ehrenberg, H.; Weitzel, H.; Fuess, H.; Hennion, B. Magnon dispersion in. *J. Phys.: Condens. Matter* **1999**, *11* (12), 2649−2659.

(22) Forsyth, J. B.; Wilkinson, C.; Zvyagin, A. I. The antiferromagnetic structure of copper tungstate, $CuWO_4$. *J. Phys.: Condens. Matter* **1991**, *3* (43), 8433−8440.

(23) Wilkinson, C.; Sprague, M. J. The magnetic structures of $NiWO_4$ and $CoWO_4$. *Zeitschrift für Kristallographie - Crystalline Materials* **1977**, *145* (1−2), 96−107.

(24) Dey, S.; Ricciardo, R. A.; Cuthbert, H. L.; Woodward, P. M. Metal-to-Metal Charge Transfer in AWO_4 (A = Mg, Mn, Co, Ni, Cu, or Zn) Compounds with the Wolframite Structure. *Inorg. Chem.* **2014**, *53* (9), 4394−4399.

(25) Ehrenberg, H.; Wltschek, G.; Trouw, F.; Kroener, T.; Weitzel, H.; Fuess, H. Magnetic structures of α-$FeMoO_4$ and α-$CoMoO_4$. *J. Magn. Magn. Mater.* **1994**, *135* (3), 355−360.

(26) Kresse, G.; Joubert, D. From ultrasoft pseudopotentials to the projector augmented-wave method. *Phys. Rev. B: Condens. Matter Mater. Phys.* **1999**, *59* (3), 1758−1775.

(27) Blöchl, P. E. Projector augmented-wave method. *Phys. Rev. B: Condens. Matter Mater. Phys.* **1994**, *50* (24), 17953−17979.

(28) Blöchl, P. E.; Jepsen, O.; Andersen, O. K. Improved tetrahedron method for Brillouin-zone integrations. *Phys. Rev. B: Condens. Matter Mater. Phys.* **1994**, *49* (23), 16223−16233.

(29) Perdew, J. P.; Ruzsinszky, A.; Csonka, G. I.; Vydrov, O. A.; Scuseria, G. E.; Constantin, L. A.; Zhou, X.; Burke, K. Restoring the Density-Gradient Expansion for Exchange in Solids and Surfaces. *Phys. Rev. Lett.* **2008**, *100* (13), 136406.

(30) Dudarev, S. L.; Botton, G. A.; Savrasov, S. Y.; Humphreys, C. J.; Sutton, A. P. Electron-energy-loss spectra and the structural stability of nickel oxide: An LSDA+U study. *Phys. Rev. B: Condens. Matter Mater. Phys.* **1998**, *57* (3), 1505−1509.

(31) Lee, A. v. d.; Beaurain, M.; Armand, P. $LiFe(MoO_4)_2$, $LiGa(MoO_4)_2$ and $Li_3Ga(MoO_4)_3$. *Acta Crystallogr., Sect. C: Cryst. Struct. Commun.* **2008**, *64* (1), i1−i4.

(32) Rodríguez-Carvajal, J. Recent advances in magnetic structure determination by neutron powder diffraction. *Phys. B* **1993**, *192* (1), 55−69.

(33) Nath, R.; Ranjith, K. M.; Roy, B.; Johnston, D. C.; Furukawa, Y.; Tsirlin, A. A. Magnetic transitions in the spin-5/2 frustrated magnet $BiMn_2PO_6$ and strong lattice softening in $BiMn_2PO_6$ and $BiZn_2PO_6$ below 200 K. *Phys. Rev. B: Condens. Matter Mater. Phys.* **2014**, *90* (2), 024431.

(34) Bramwell, S. T.; Holdsworth, P. C. W. Magnetization and universal sub-critical behaviour in two-dimensional XY magnets. *J. Phys.: Condens. Matter* **1993**, *5* (4), L53−L59.
(35) Neaton, J. B.; Ederer, C.; Waghmare, U. V.; Spaldin, N. A.; Rabe, K. M. First-principles study of spontaneous polarization in multiferroic $BiFeO_3$. *Phys. Rev. B: Condens. Matter Mater. Phys.* **2005**, *71* (1), 014113.

https://dx.doi.org/10.1021/acs.inorgchem.0c00432
Inorg. Chem. 2020, 59, 8127−8133